Supplementary Information

CVD Synthesis of Carbon Spheres using NiFe-LDHs as Catalytic Precursors. Structural, electrochemical and magnetoresistive properties.

Jose A. Carrasco,[a] Helena Prima-Garcia,[a] Jorge Romero,[a] Jesús Hernández-Saz,[b] Sergio I. Molina,[b] Gonzalo Abellán,[a,c,]* and Eugenio Coronado[a,]*

[a] *Instituto de Ciencia Molecular (ICMol), Universidad de Valencia, Catedrático José Beltrán 2, 46980, Paterna, Valencia, Spain.*

[b] *Departamento de Ciencia de los Materiales e Ingeniería Metalúrgica y Química Inorgánica, IMEYMAT, Universidad de Cádiz, 11510 Puerto Real, Cádiz, Spain.*

[c] *Department of Chemistry and Pharmacy and Institute of Advanced Materials and Processes (ZMP), University Erlangen-Nürnberg, Henkestr. 42, 91054 Erlangen and Dr.-Mack Str. 81, 90762 Fürth, Germany.*

Contents

SI 1. Characterization of carbon spheres before the annealing process.

SI 1.1. FESEM and HRTEM microscopy.

(A) Selected FESEM image of the original (before the thermal treatment) carbon spheres. (B) HRTEM showing the chain-like disposition due to accretion effects. (C) Histogram of 50 spheres displaying the average diameter taken from FESEM images.

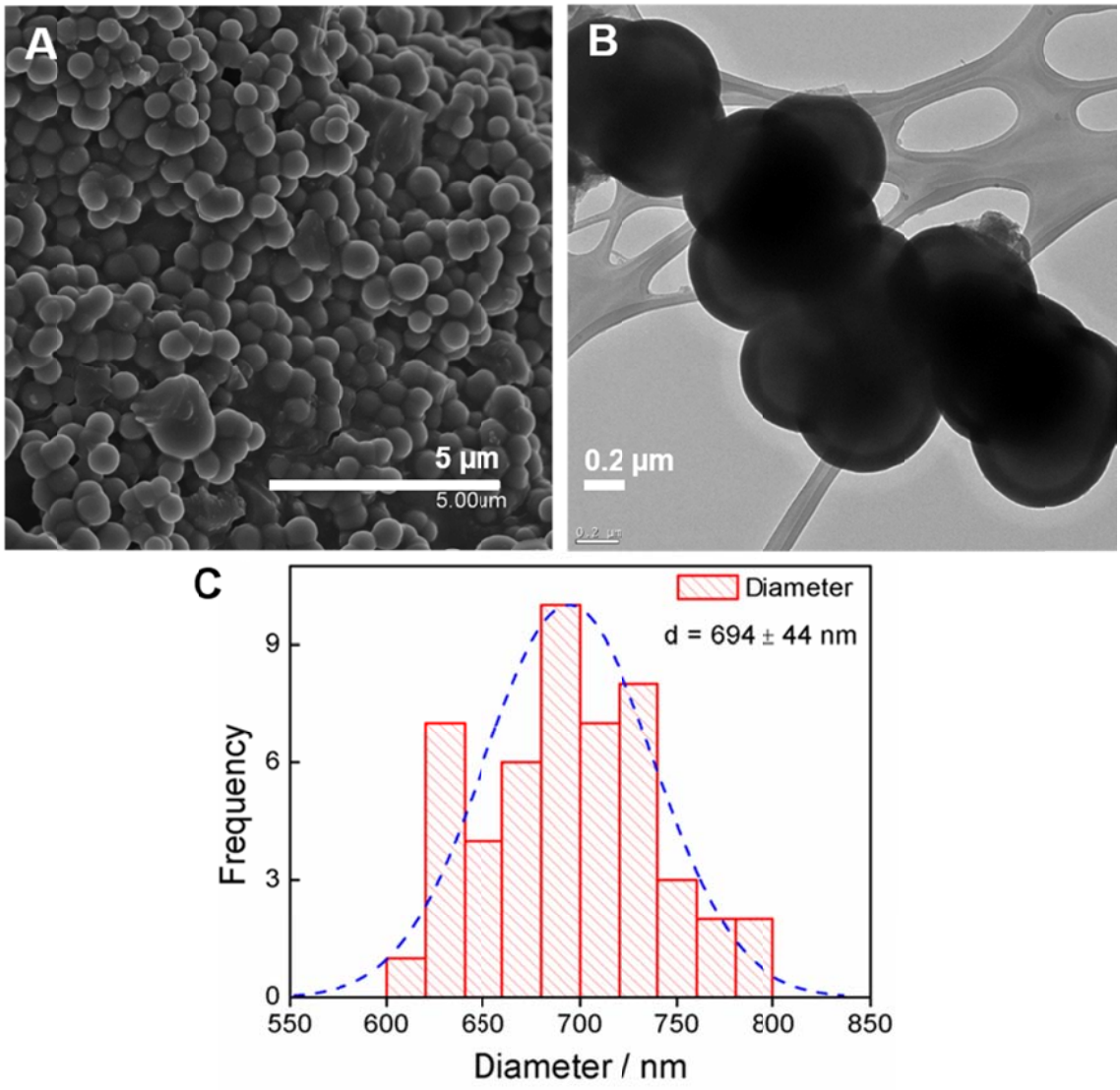

SI 1.2. XRPD.

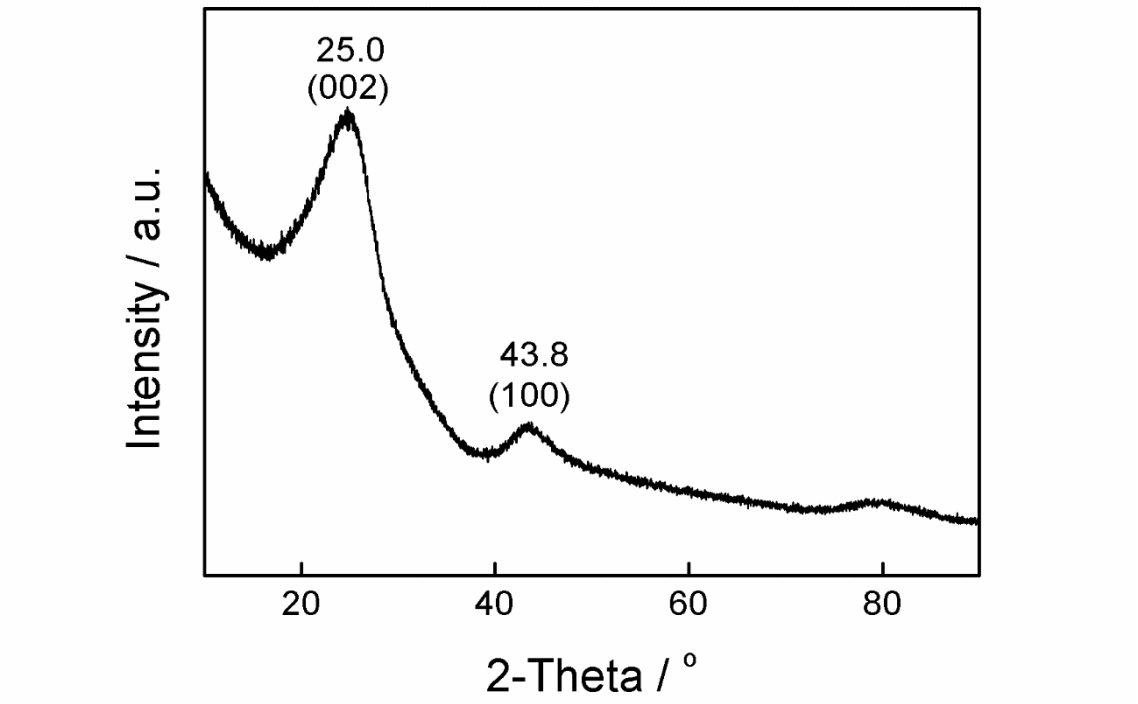

SI 1.3. Thermogravimetric analysis (TGA) in air and N_2.

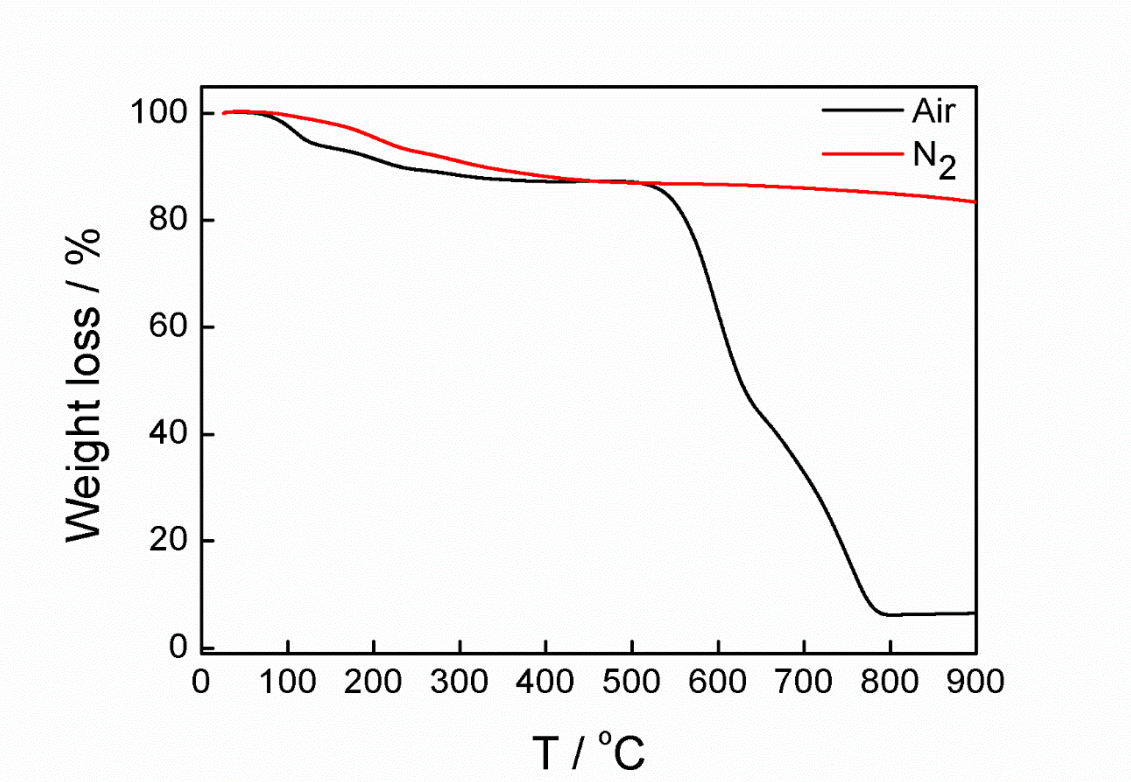

In air atmosphere, the combustion temperature of *ca.* 595 ^{o}C, as obtained from the DTA, is in good agreement within the range of carbon nano-spheres based on the classification of Serp *et al*. according to the maximum of gasification rate.[1]

SI 2. Characterization of control experiments.

SI 2.1. Calcination of NiFe-LDH.

A control experiment at 900 ^{o}C with a scan rate of 5 ^{o}C·min^{-1} was carried out in absence of ethylene (therefore only supplying H_2 as the reducing agent) to elucidate the species formed after the calcination procedure. The following XRPD spectrum compares both the pristine and the calcined LDH:

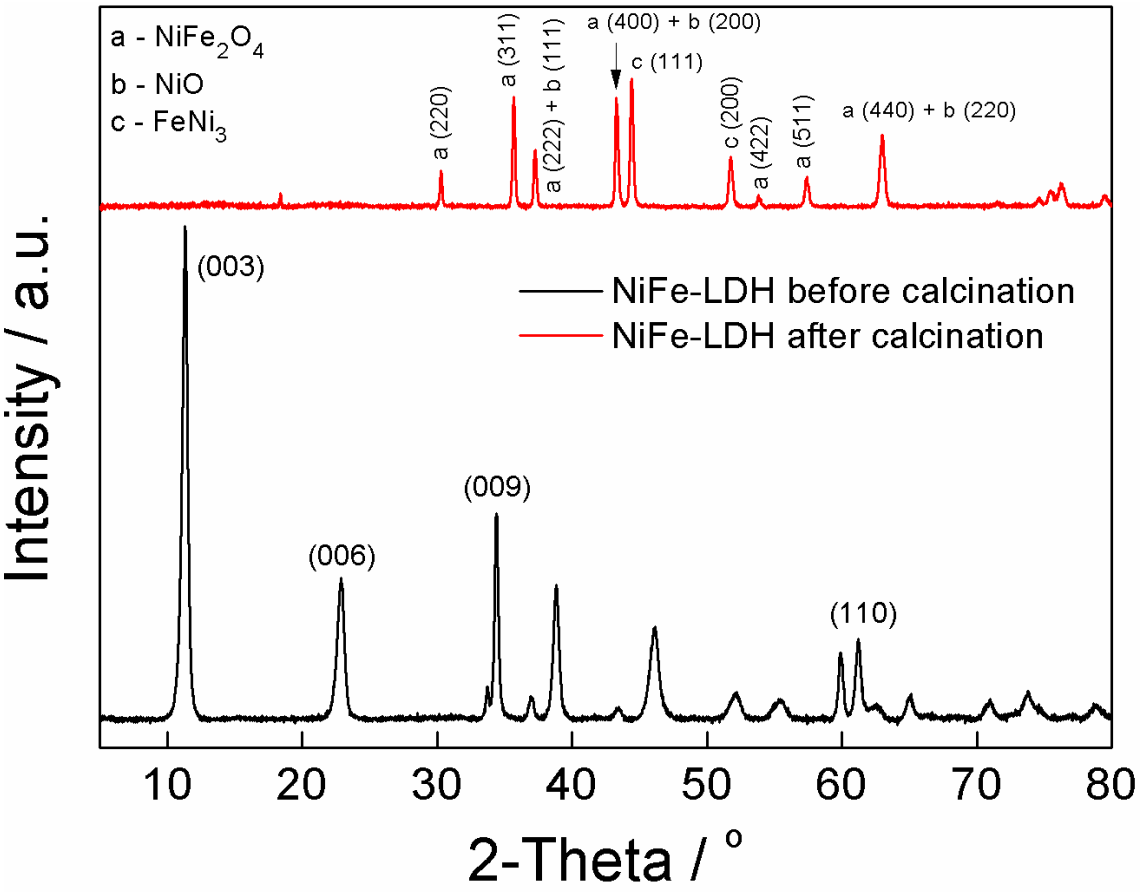

The spectra exhibit the formation of a mixture of three phases: $NiFe_2O_4$, NiO and $FeNi_3$ alloy.

Another control experiment in absence of both H_2 and C_2H_4 only depicts the presence of $NiFe_2O_4$ and NiO:

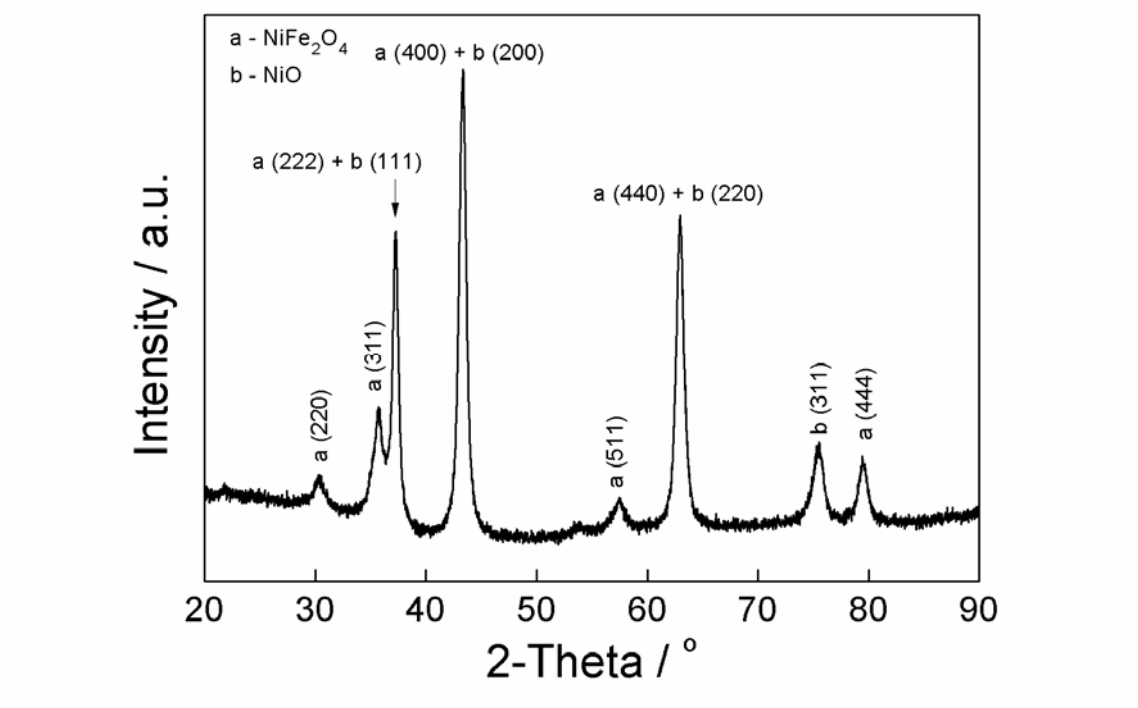

Since the $FeNi_3$ alloy only appears in the presence of a reduction agent, we can conclude that is the main catalytic specie responsible for the carbon nanoform growing. For further information in the characterization and study of related control experiments, see ref [2].

SI 2.2. Carbon Spheres

SI 2.2.1. FESEM microscopy.

Both images depict the formation of carbon spheres with a wide range of diameters, from *ca.* 700 – 800 nm for the smallest ones to several microns for the biggest spheres. The latter ones are formed by accumulation effects, displaying a caterpillar-like morphology.

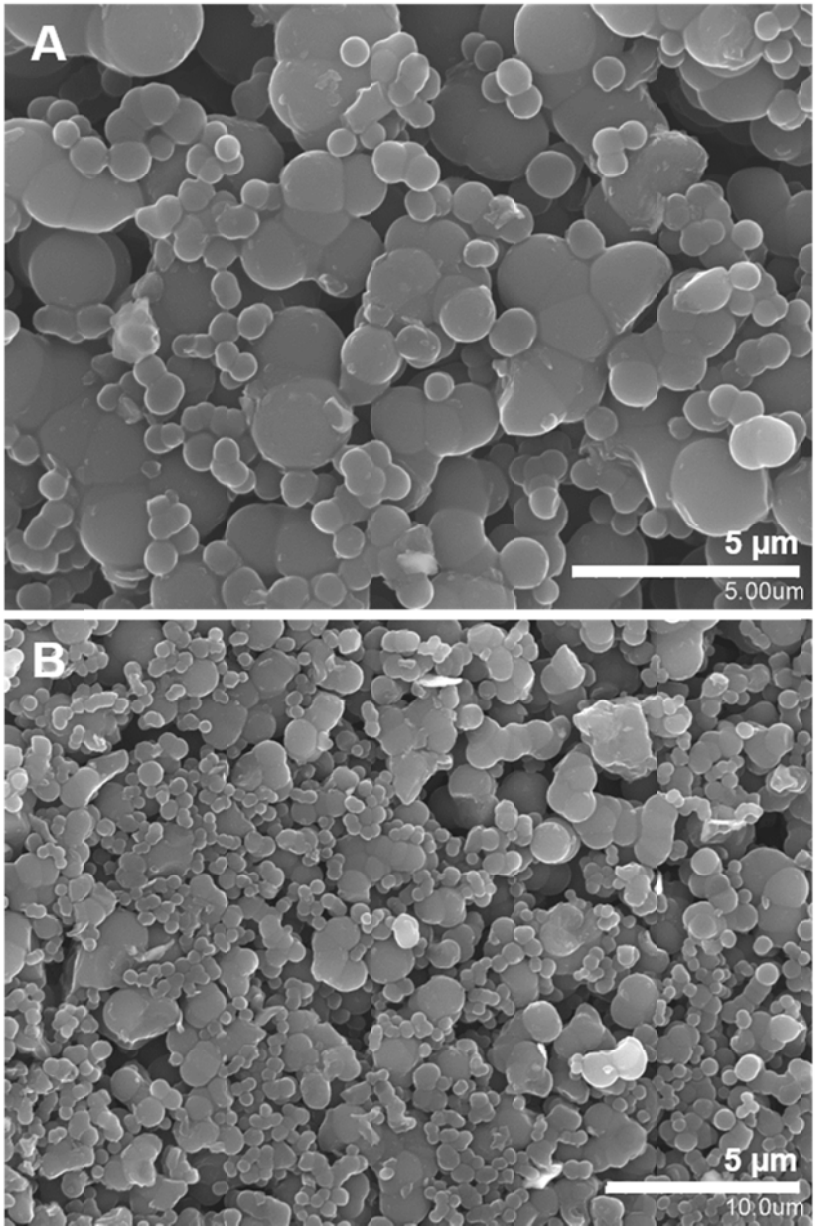

SI 2.2.2. XRPD

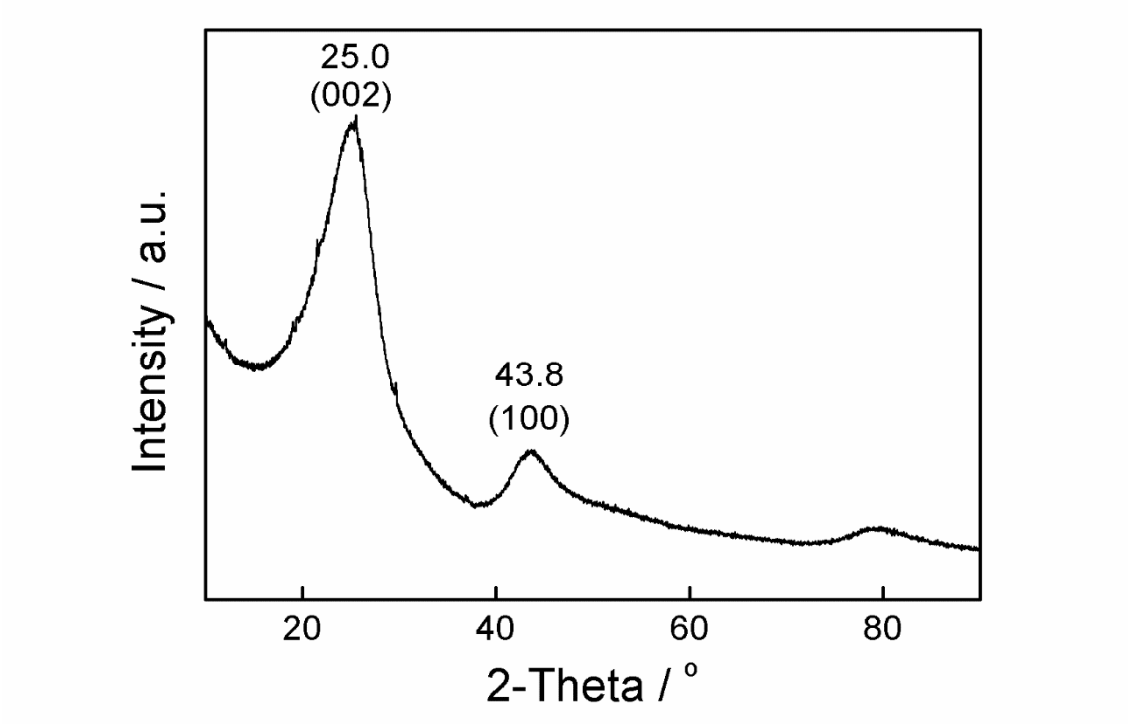

SI 2.2.3. Thermogravimetric analysis (TGA) in air and N_2.

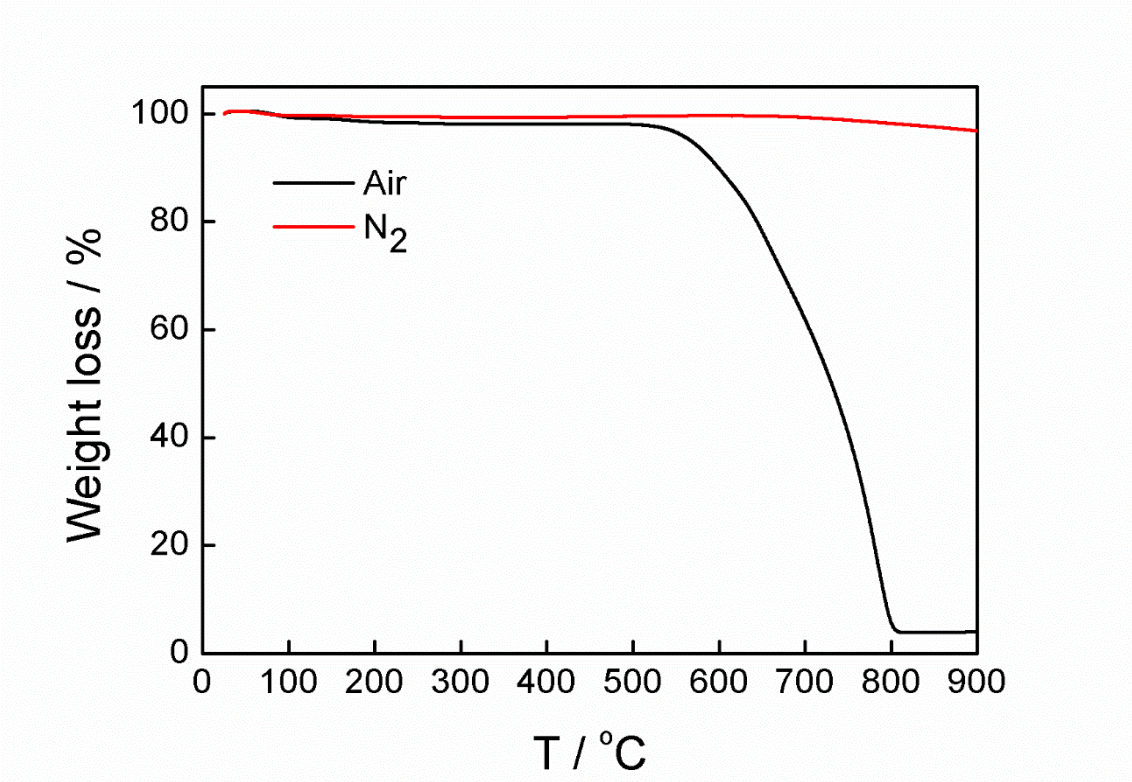

The combustion temperature of *ca.* 600 ^{o}C in air atmosphere (obtained from the DTA), is in good agreement within the range of carbon nano-spheres according to the classification of Serp *et al*. on the basis of the maximum of gasification rate.[1]

SI 3. Raman spectra comparison.

Raman spectra for (a) the control experiment at 900 ^{o}C and the carbon spheres (b) before and (c) after the thermal treatment at 800 ºC. All spectra for the different samples display two peaks centered at *ca.* 1354 and 1600 cm^{-1}, related with the D (disorder) and G (order) band, and an I_D/I_G of *ca.* 0.8.

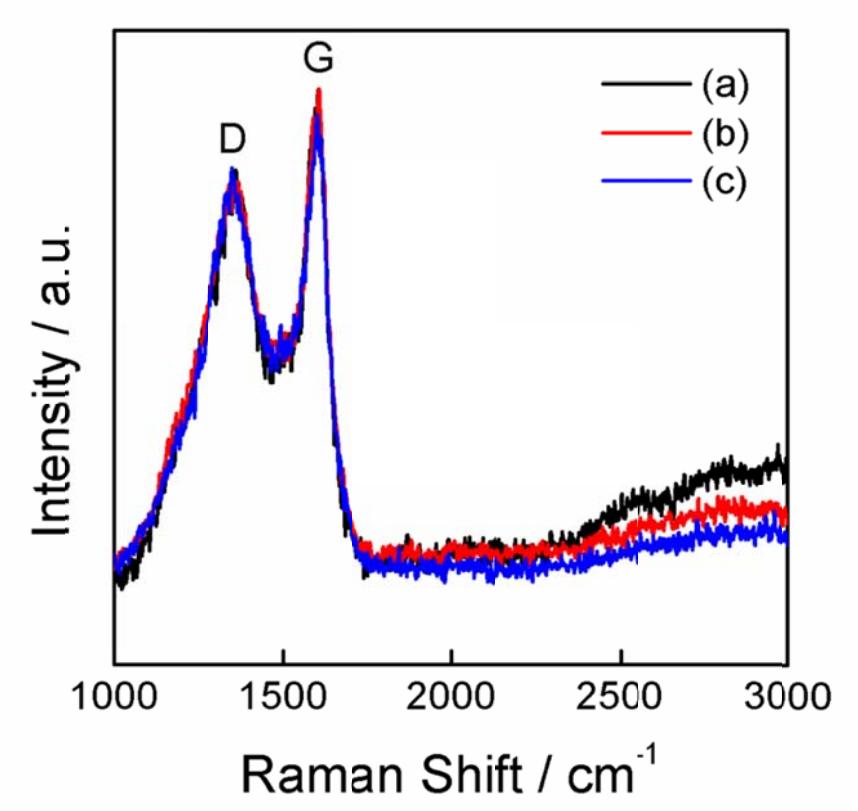

SI 4. DTA analysis of CS in air.

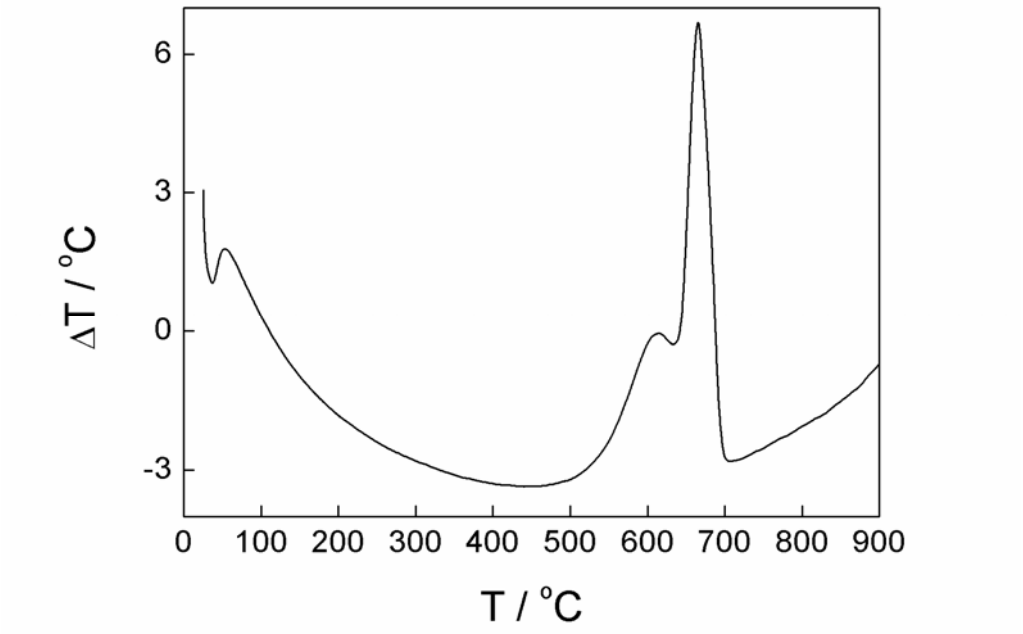

SI 5. Additional microscopy images of CS and accretion effects.

(A) FESEM image showing the average diameter of the spheres of *ca.* 700 – 800 nm, as depicted in the main article. (B) FESEM image in low magnification (3000x) displaying a large selected area of carbon spheres and highlighting some bigger spheres formed by an accretion process. The average diameter of the accreted carbon spheres is about 1.5 – 2.0 µm. (C) FIB-SEM image showing a milled region. (D) FIB-SEM cross-section image of the same region of (C) depicting the solid inner structure.

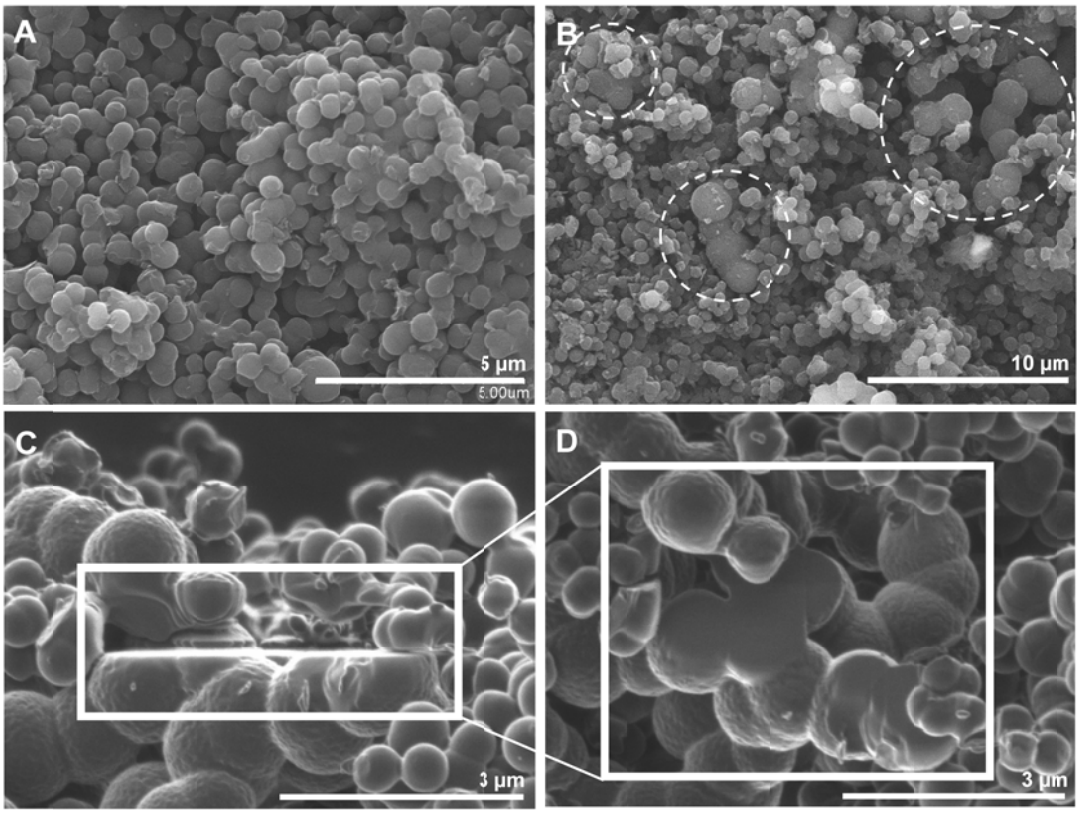

SI 6. XPS of carbon spheres.

SI 6.1. XPS of carbon spheres synthesized at 900 ^{o}C and 1000 ^{o}C.

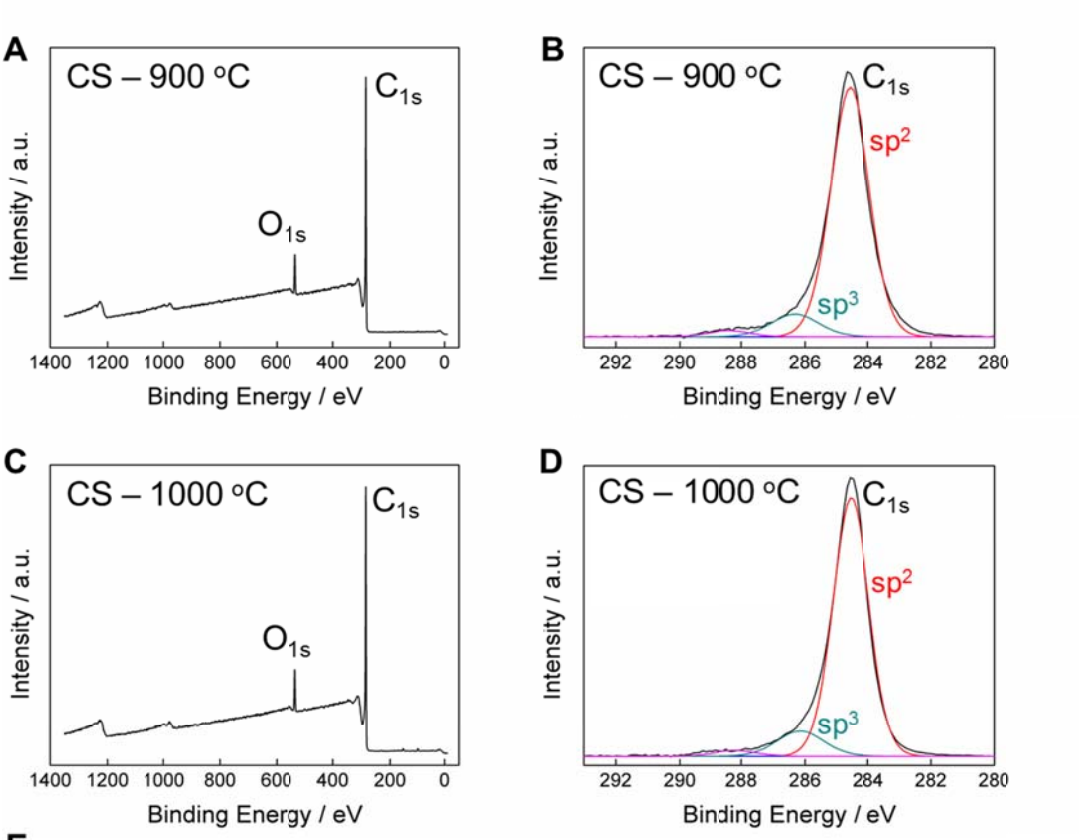

E

Atomic %	CS – 900 °C	CS – 1000 °C
C	91,66	92,68
N	0,36	0,24
O	7,98	7,09

(A) Survey and (B) C_{1s} spectrum of carbon spheres synthesized at 900 ^{o}C. (C) Survey and (D) C_{1s} spectrum of carbon spheres synthesized at 1000 ^{o}C. (E) Comparative table with atomic percentages between both spheres.

SI 6.2. XPS spectra of the Fe 2p and Ni 2p core-levels in **CS** (900 ^{o}C).

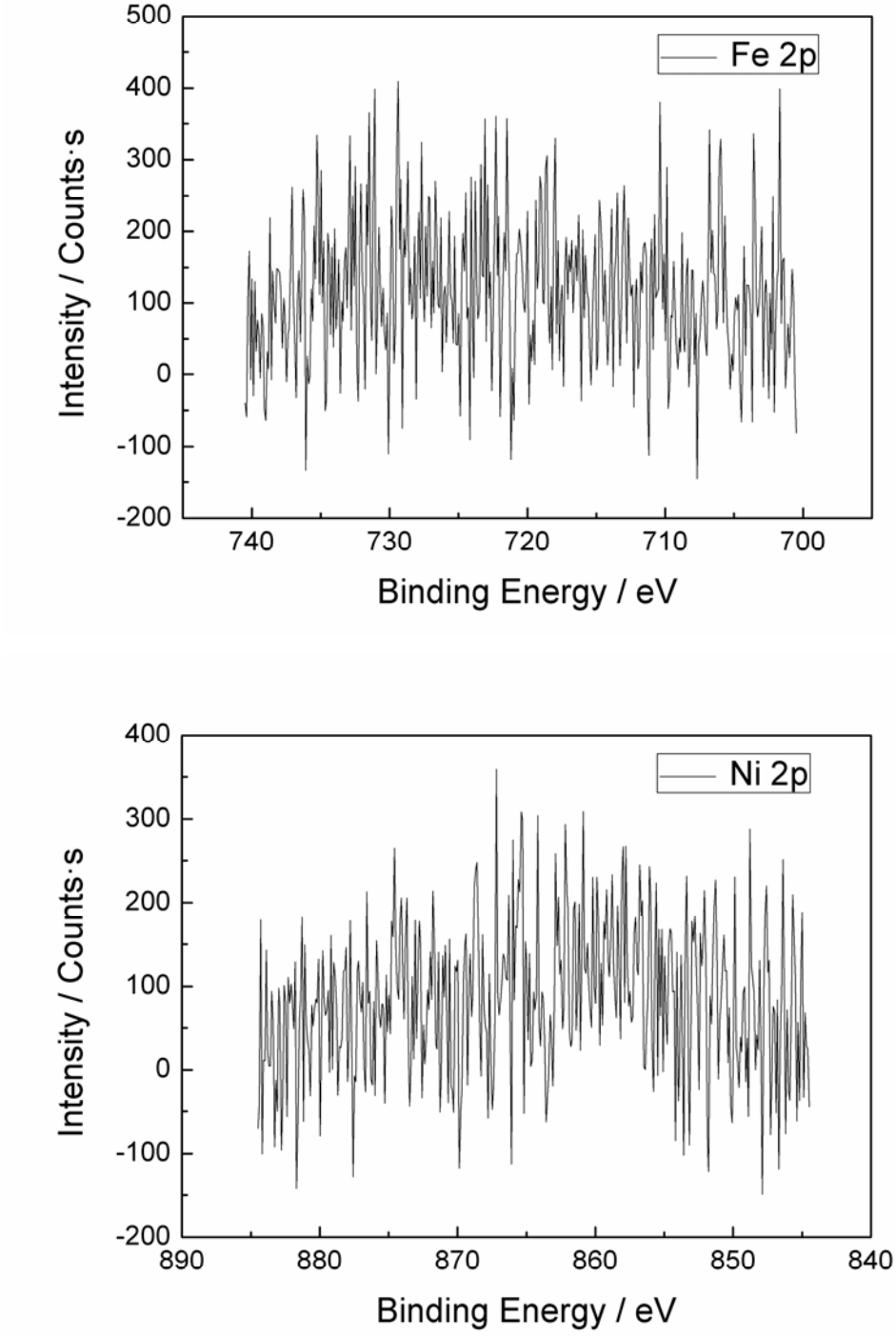

SI 7. FIB-SEM sequential steps of the lift-out procedure.

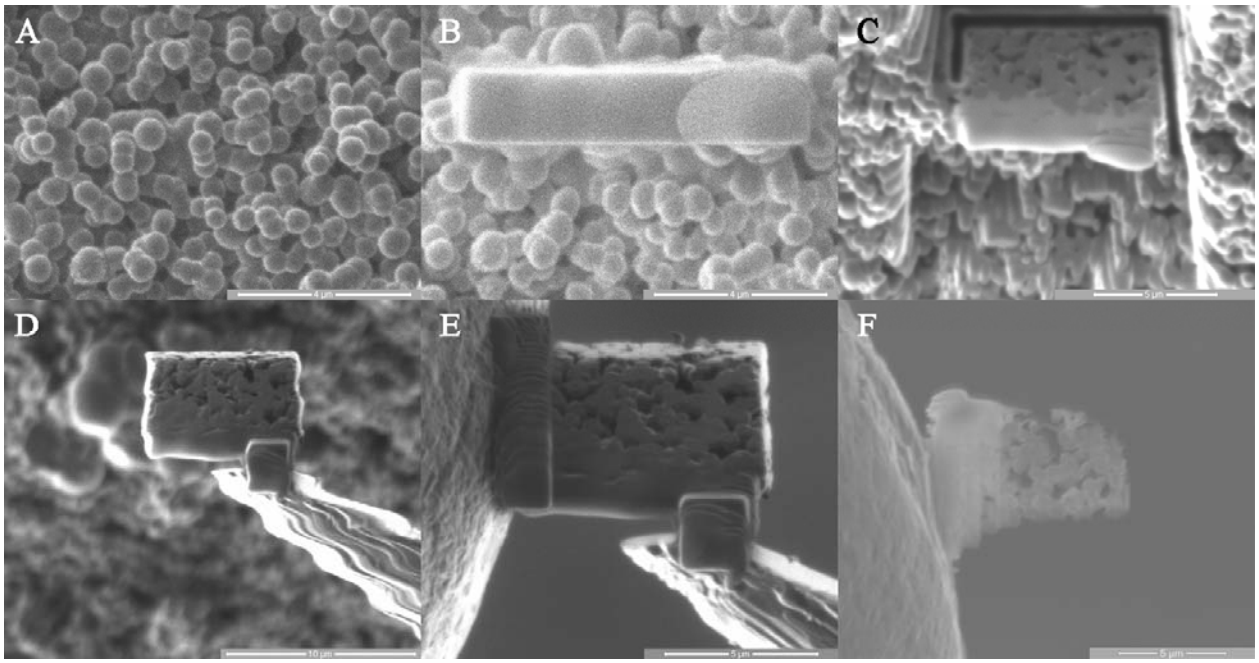

(A) select a localization, (B) deposit a platinum layer, (C) mill trenches (tilted view), (D) lamella attached to the micromanipulator, (E) lamella attached to the TEM grid and the micromanipulator and (F) lamella thinned down to electron-transparency. From (A) to (E) are FIB images and (F) is a SEM image.

SI 8. Differential pore volume distribution by DFT of CS.

DFT method summary

Pore volume = 0.009 $cc \cdot g^{-1}$

Surface area = 14.684 $m^2 \cdot g^{-1}$

Lower confidence limit = 10.960 Å

Fitting error = 0.410 %

Pore width (Mode) = 10.960 Å

The model which has been used is "QSDFT-N_2-carbon adsorption branch at 77 K based on a slit/cylinder pores" obtained from www.quantachrome.com/technical/dft.html, and in good agreement with similar samples in literature.[3,4] Differential pore volume distribution by DFT is represented in the following plot:

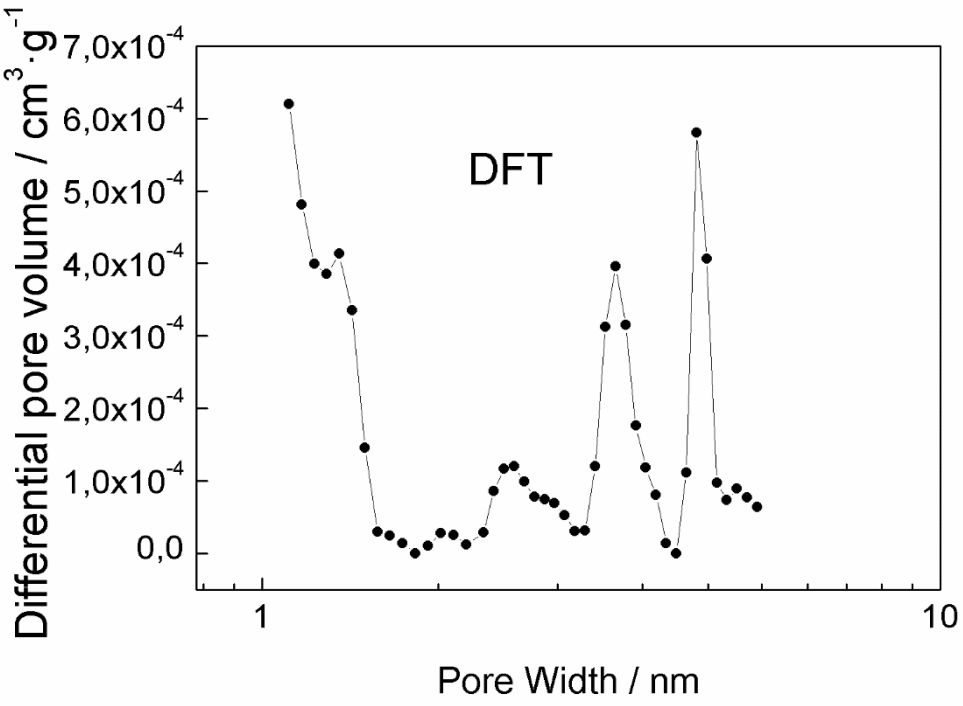

The low value of pore volume suggests the presence of ultramicropores. [3,4]

SI 9. Electrochemical properties of carbon spheres synthesized at 1000 ^{o}C.

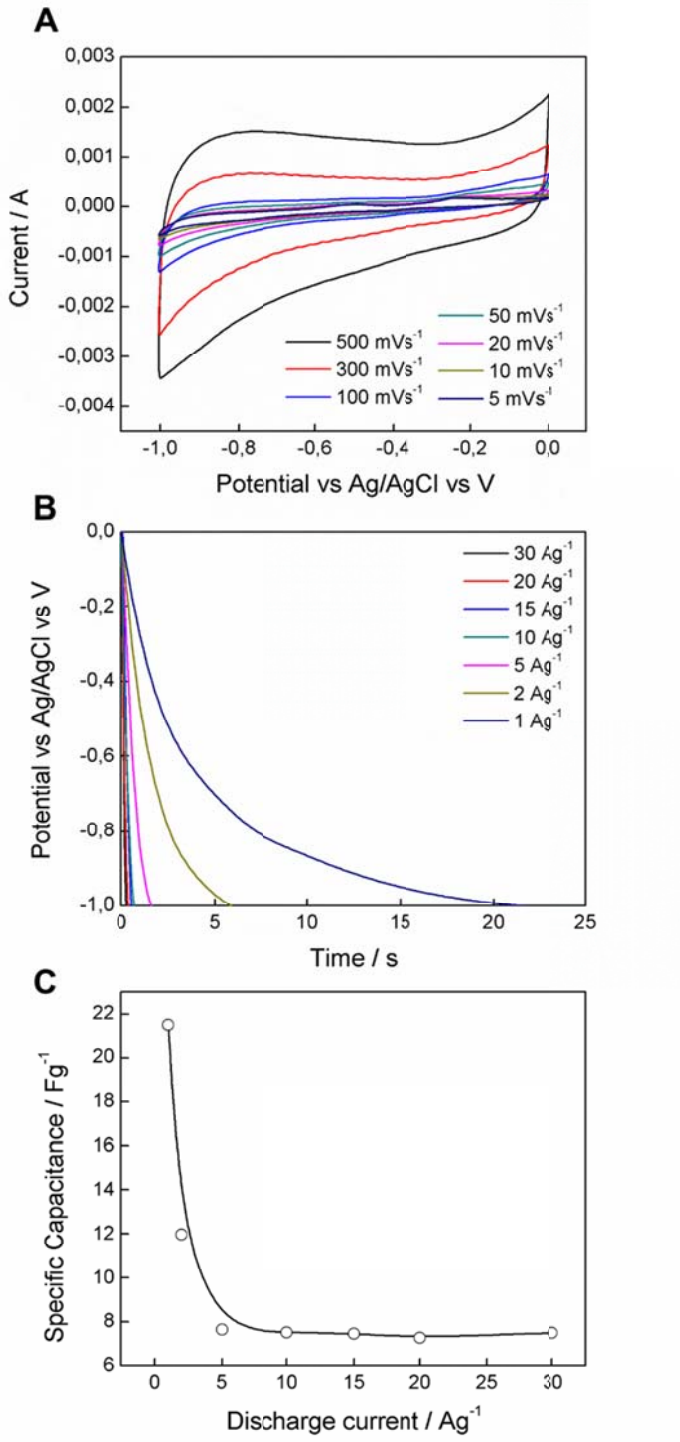

(A) CV curve at various scan rates in a 6 M KOH aqueous solution. (B) Galvanostatic discharge curves at different discharge current densities. (C) Specific capacitance of the material at different discharge current densities.

SI 10. Fit the magnetoresistance curves with the relation MR ∝ $(\mu_0 \cdot \mu \cdot |H|)^2$.

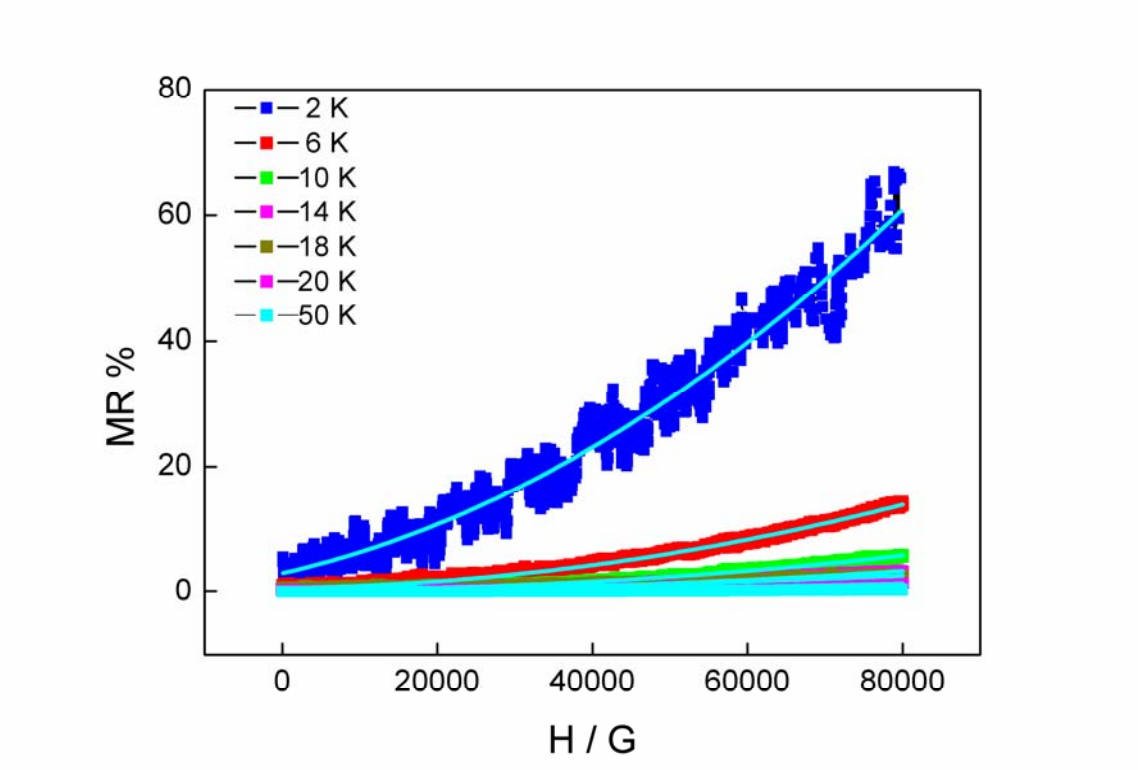

SI 11. Magnetic temperature dependence of CS.

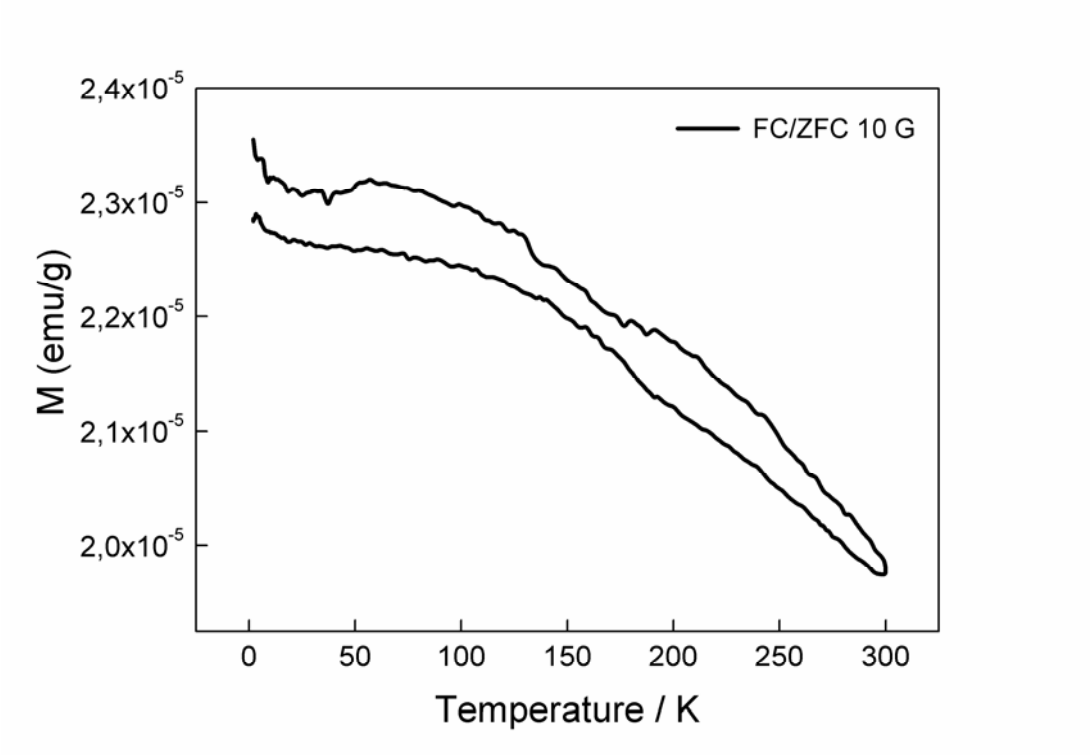

SI 12. Magnetoresistance dependence with the temperature.

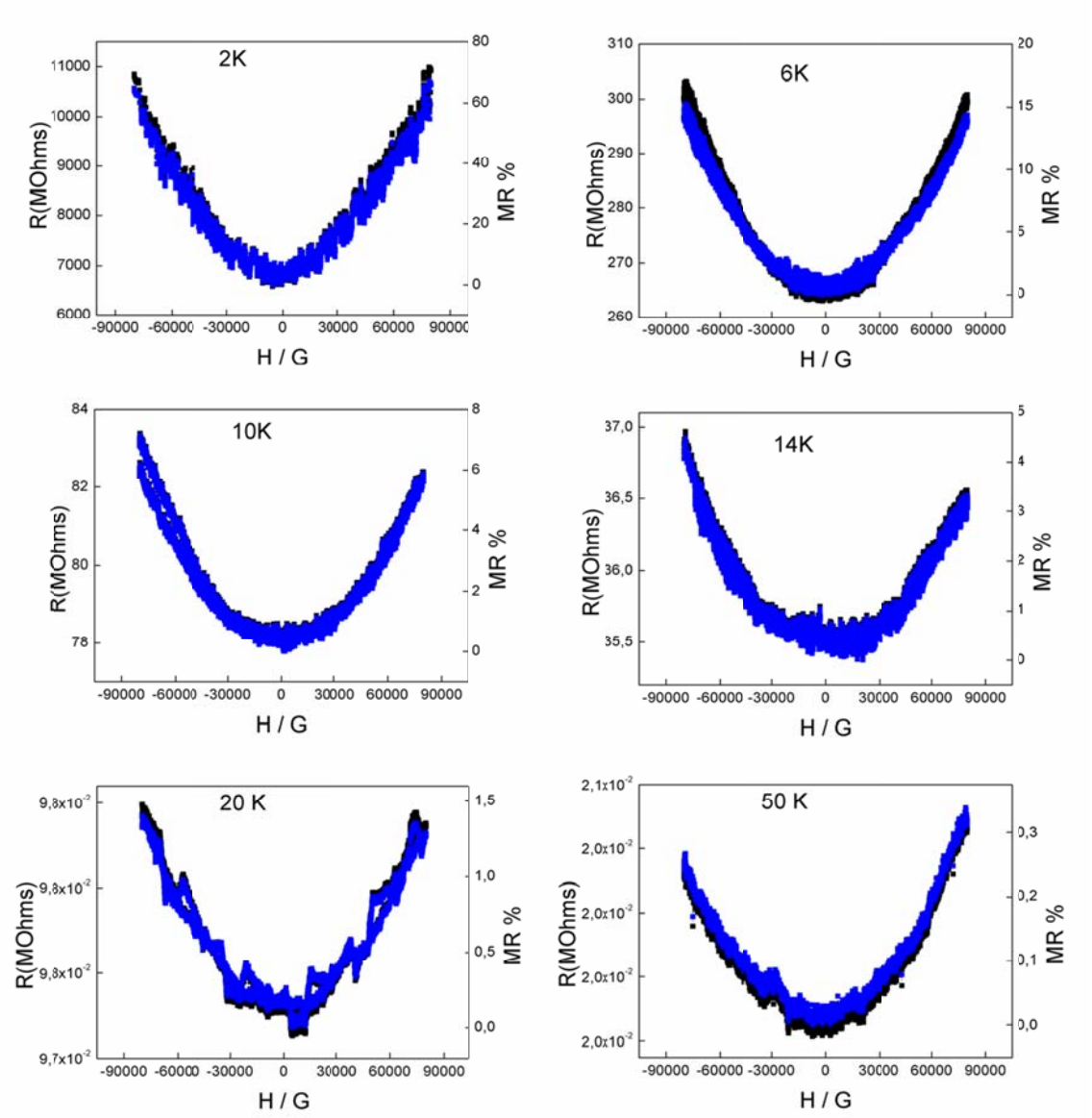

SI 13. Additional References.

1 P. Serp, R. Feurer, P. Kalck, Y. Kihn, J. L. Faria and J. L. Figueiredo, *Carbon*, 2001, **39**, 621–626.

2 G. Abellán, J. A. Carrasco, E. Coronado, J. P. Prieto-Ruiz and H. Prima-García, *Adv. Mater. Interfaces*, 2014, **1**, 1400184.

3 Y. Han, X. Dong, C. Zhang and S. Liu, *J. Power Sources*, 2012, **211**, 92–96.

4 N. P. Wickramaratne, J. Xu, M. Wang, L. Zhu, L. Dai and M. Jaroniec, *Chem. Mater.*, 2014, **26**, 2820–2828.